




Tuning luminescent properties of a metal organic framework by insertion of metal complexes

Youssef Atoini, Eko Adi Prasetyanto, Pengkun Chen, Dries Jonckheere, Dirk De Vos & Luisa De Cola


To cite this article: Youssef Atoini, Eko Adi Prasetyanto, Pengkun Chen, Dries Jonckheere, Dirk De Vos & Luisa De Cola (2017): Tuning luminescent properties of a metal organic framework by insertion of metal complexes, *Supramolecular Chemistry*, DOI: [10.1080/10610278.2017.1290249](https://doi.org/10.1080/10610278.2017.1290249)


To link to this article: <http://dx.doi.org/10.1080/10610278.2017.1290249>

 View supplementary material 

 Published online: 20 Feb 2017.

 Submit your article to this journal 

 Article views: 26

 View related articles 

 View Crossmark data 

Tuning luminescent properties of a metal organic framework by insertion of metal complexes

Youssef Atoini^a, Eko Adi Prasetyanto^a, Pengkun Chen^a, Dries Jonckheere^b, Dirk De Vos^b and Luisa De Cola^a

^aInstitut de Science et Ingénierie Supramoléculaires (ISIS – UMR 7006), Université de Strasbourg & CNRS, Strasbourg, France; ^bCentre for Surface Chemistry and Catalysis, KU Leuven – University of Leuven. Leuven Chem&Tech, Leuven, Belgium

ABSTRACT

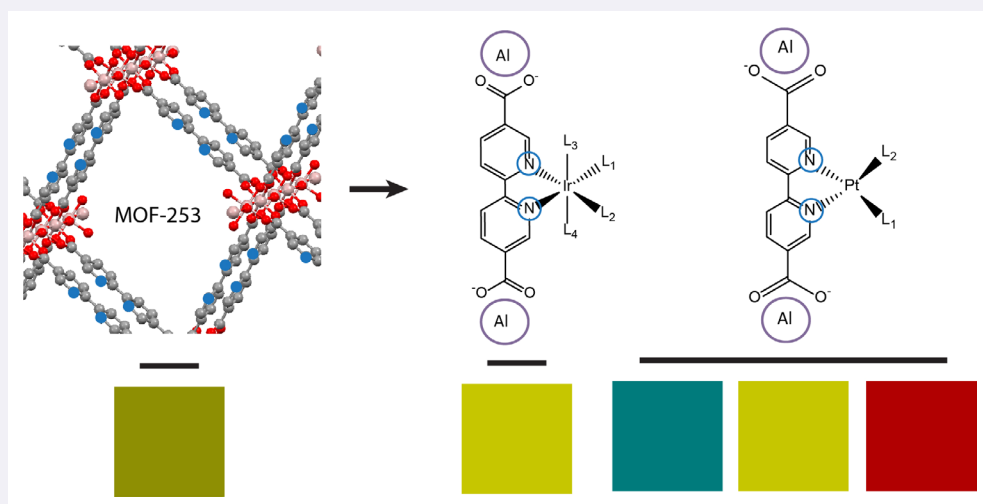
We report the preparation and characterisation of new emissive materials based on the insertion of platinum(II) and iridium(III) complexes inside the Al(OH)(bipyridine dicarboxylate) metal organic framework (MOF-253). Guest incorporation is performed by coordination of a metal complex precursor, and provides increased robustness to the system compared to guest inclusion by its physical diffusion. Powder X-ray diffraction analysis highlights the high degree of crystallinity of the materials, with a complete change in the lattice parameters upon metal complex insertion. The photophysical properties of the resulting materials were thoroughly investigated. This synthetic approach is particularly attractive since, as we show, it is possible to tune the emission maxima of our materials over the entire visible range.

ARTICLE HISTORY

Received 23 November 2016
Accepted 28 January 2017

KEYWORDS

MOF; metal complexes;
luminescence; photophysical
properties



1. Introduction

Metal Organic Frameworks (MOFs), also known as Porous Coordination Polymers (PCPs), are an emerging class of complexes in which coordination bonds between one or several metal centres and organic moieties, known as ligands or linkers, create geometrically well-defined and highly crystalline structures (1). Up to now, several hundreds of MOFs have been reported (2, 3) MOFs feature straightforward syntheses, nanoscale process ability, predictable structures and network geometry, possibility

of post-synthetic modification and in most cases, a relatively tuneable porosity (with the exception of 0D and 1D MOFs) (4) Due to these characteristics, these types of hybrid organic–inorganic materials are attracting growing interest. They are widely studied in gas separation (5), gas storage (6, 7), medicine (8–11), catalysis (12) and optoelectronics (13).

Notwithstanding the availability of structural and chemical data on MOFs, their photophysical properties are rarely addressed. Indeed, only about 15% of the reported MOFs are described as luminescent, even though

CONTACT Luisa De Cola ✉ decola@unistra.fr; Eko Adi Prasetyanto ✉ prasetyanto@unistra.fr

Supplemental data for this article can be accessed at <http://dx.doi.org/10.1080/10610278.2017.1290249>

this figure has been increasing steadily over the last few years (14, 15) and they mainly involve rare earth elements (16, 17). Like their molecular counterparts, organometallic complexes, excited MOFs can relax through both fluorescence and phosphorescence. Moreover, the luminescence may result from ligand-centred (LC) transitions, ligand to metal charge transfer (LMCT) or metal to ligand charge transfer (MLCT) phenomena (18).

As mentioned above, the porosity of MOFs implies the possibility to encapsulate guest molecules inside the pores themselves. However, for most systems, the insertion is performed only physically by guest diffusion into the bulk structure. In 2013, Li et al. demonstrated the production of white light by incorporation of yellow emissive iridium complex inside blue emissive MOF (19). Despite the efficiency of this material, the complex is not linked to the framework by a real chemical bond, but held in the anionic framework after diffusion inside the host materials, like for inorganic porous materials such as zeolites (20), mesoporous silica nanoparticles (21) or calcite (22). The latest approach to overcome this problem is the construction of MOFs, with a linker bearing several coordination sites. Figure 1 represents 22'-Bipyridine-55'-dicarboxylic acid (bpydc), a common organic linker used in MOF synthesis, including for MOF-253 used in this work. Primary binding sites of the linker form the structure of the MOF itself, while the secondary binding sites could be used for additional host-guest interactions. Those interactions depend on the nature of the binding site involved (hydrogen bonding (23) electrostatic interaction, π - π stacking (24), covalent bond (25), coordination bond (26), etc.). The use of coordination bonds is particularly important for metal complex insertion. This incorporation method of metal complexes in MOF-253 is widely used for catalysis or gas uptake, but so far has not been explored for luminescence purposes. Indeed, in the first report on MOF-253, Yaghi et al. investigated the insertion of PdCl₂ and Cu(BF₄)₂ in order to demonstrate the selectivity factor for binding CO₂ over N₂ under typical flue gas conditions (27). Further research involved metal insertion for catalysed reactions such as alcohol oxidations (28), arylations (29) or couplings (30).

Thanks to their luminescent properties, metal complexes of transition metals such as iridium (III) or platinum (II) are very good candidates for optoelectronic applications (31). They feature high stability, high emission quantum yields, tunable energy of the emission and, due to the triplet nature of the luminescent state, long excited-states lifetimes.

In the case of platinum complexes, favoured by their square planar geometry, there is a possibility of aggregation promoted by metallophilic and π - π stacking interactions (32-34). Therefore, they provide a tuneable emission behaviour according to the stacking and the investigation

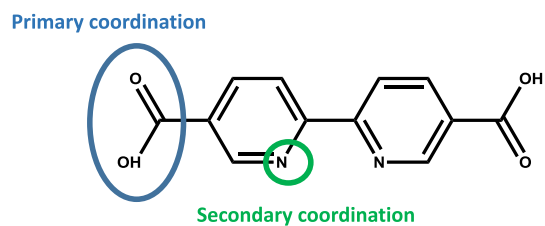


Figure 1. (Colour online) Representation of bpydc, showing primary and secondary coordination sites.

of Pt(II) complexes has taken more and more space in the luminescence field.

In this work, we report the synthesis and characterisation of MOF-253 and incorporation of transition metal complexes (TMCs) by a robust coordination with a chelating ligand. The resulting MOF-metal complexes have been investigated and their photophysical behaviour is described.

2. Synthesis and characterisation

2.1. Synthesis

2.1.1. Synthesis of MOF-253

The synthesis of MOF-253 was performed according to O. Yaghi et al. (27). A solution of AlCl₃·6H₂O (302 mg, 1.25 mmol) and glacial acetic acid (1.7 mL, 30.0 mmol) in 20 mL N,N'-dimethylformamide was added to a Teflon-capped vial containing 22'-bipyridine-55'-dicarboxylic acid (306 mg, 1.25 mmol). The mixture was heated on a hot plate at 120 °C for 24 h. The resulting white crystalline powder was subsequently filtered and washed with DMF and with methanol by Soxhlet extraction for 24 h, collected by filtration and dried under vacuum on a Schlenk line for 24 h to yield a white crystalline powder. The final material was characterised by Thermogravimetric analysis, Powder X-ray diffraction, X-ray photoelectron spectroscopy, Nitrogen adsorption-desorption, Transmission electron microscopy.

2.1.2. The metal complex precursors

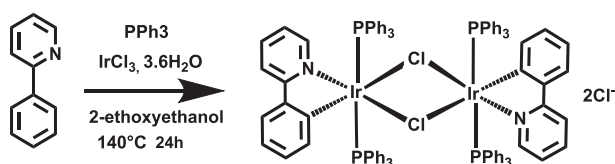
All platinum precursors ((22'-bipyridine) dichloro-platinum(II) (**MOF-Pt1** precursor), cis-dichlorobis(triphenylphosphite) platinum(II) (**MOF-Pt2** precursor), cis-dichlorobis(triphenylphosphine)platinum(II) (**MOF-Pt3** precursor)), were purchased from Sigma-Aldrich and Alfa Aesar. The iridium starting material, IrCl₃ was bought from Metal Precious Online and the iridium dimers have been synthesised according to previous procedures (35-37). The characterisation data of the precursors are shown in the Supplemental material (Figure S2-S8) (Scheme 1).

To obtain **Ir1** precursor, Iridium trichloride hydrate (181 mg, 0.5 mmol), 2-phenylpyridine (233 mg, 1.5 mmol)

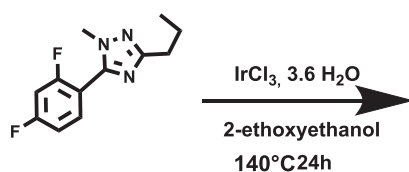
and triphenylphosphine (393 mg, 1.5 mmol) were added into a mixture of 2-ethoxyethanol and water (3:1) and the reaction media was refluxed and stirred under nitrogen atmosphere for 12 h and then cooled to room temperature. The obtained yellow precipitate was filtered and washed with water and ethanol several times and purified by column chromatography on silica gel with dichloromethane/ethyl acetate (5:1) as solvent to give a pale yellow solid. (0.35 mg, 0.37 mmol, 74%). $^1\text{H NMR}$ (400 MHz, CD_2Cl_2) δ [ppm] = 9.15 (m, 1H), 8.65 (m, 1H), 8.42 (m, 1H), 8.00 (m, 2H), 7.67 (m, 2H), 7.24 (m, 17H); $^{31}\text{P NMR}$ (160 MHz, CD_2Cl_2): 29.9 (Scheme 2).

To obtain **Ir2** precursor, Iridium trichloride hydrate (0.3 g, 0.82 mmol) and 5-difluorophenyl-1-methyl-3-propyl-124-triazole (dfptz) were added into a mixture of 2-ethoxyethanol and water (3:1) and the reaction was refluxed and stirred under nitrogen atmosphere for 12 h and then cooled to room temperature. The obtained slight yellow solid was filtered and washed with water and ethanol (0.89 g, 0.64 mmol, 78%). $^1\text{H NMR}$ (400 MHz, CDCl_3) δ [ppm] = 6.31 (m, 1H), 5.50 (m, 1H), 4.18 (m, 3H), 2.38 (m, 1H), 1.85 (m, 1H), 1.39 (m, 1H), 1.20 (m, 5H); $^{19}\text{F NMR}$ (375 MHz, CDCl_3): -104, -107. ESI-MS (m/z): [M + H]⁺ found 665.1621 (referring to $\text{Ir}(\text{dfptz})_2$ of the dimer due to stability of the product in the MS) (Scheme 3).

To obtain **Ir3** precursor, Iridium trichloride hydrate (0.5 g, 1.40 mmol) was combined with 2-phenylpyridine (ppy) (0.8 mL, 5 mmol) in 40 mL of a mixture of 2-ethoxyethanol and water (3:1). And reflux for 24 h. The solution was cooled to room temperature, and the yellow precipitate was collected on a glass filter frit. The precipitate was washed with water, ethanol and diethylether. The solid was dissolved in dichloromethane (50 mL) and filtered, which was then concentrated under vacuum and cooled to give



Scheme 1. Synthetic pathway of Iridium precursor (**Ir1**).



Scheme 2. Synthetic pathway of Iridium precursor (**Ir2**).

dark yellow crystals and dark yellow powder of $[\text{Ir}(\text{ppy})_2\text{Cl}_2]_2$, (1.18 g, 1.1 mmol, 80%). $^1\text{H NMR}$ (400 MHz, CD_2Cl_2) δ [ppm] = 9.30 (m, 2H), 7.99 (m, 2H), 7.84 (m, 2H), 7.61 (m, 2H), 6.88 (m, 4H), 6.65 (m, 2H), 5.92 (m, 2H); ESI-MS (m/z): [M + H]⁺ found 501.0941 (referring to $\text{Ir}(\text{ppy})_2$ due to stability of the product in the MS).

2.1.3. Metal complex insertion in the MOF-253

To a dispersion of the metal complex precursor (0.09625 mmol), in 10 mL of toluene, was added **MOF-253** (25 mg, 0.0875 mmol). The mixture was stirred at 90 °C for 24 h, and cooled down to 0 °C. The resulting precipitate was filtered under vacuum, washed twice with toluene, water and ethanol and dried under vacuum to yield the final material. (Scheme 4)

2.2. Synthesis of (Pt(II))bisbipyridine dichloride

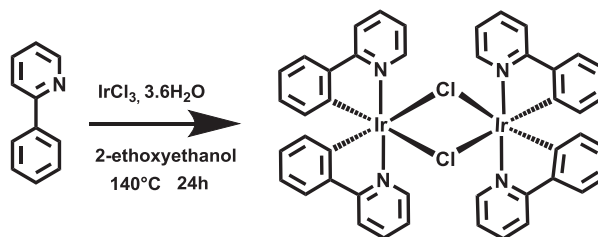
To a dispersion of (22'-bipyridine) dichloroplatinum(II) in toluene was added bipyridine dicarboxylate. The reaction mixture was stirred at 100 °C overnight. The resulting precipitate was dried under reduced pressure and purified by column chromatography on silica gel (eluent: CH_2Cl_2 9:1 MeOH) to afford the final compound.

2.2.1. Photophysical characterisation

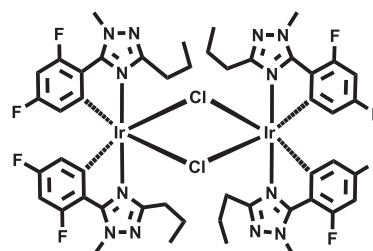
All the photophysical characterisation was done in solid stated under aerated condition at room temperature. Detailed information about the technique is provided in the Supplemental material.

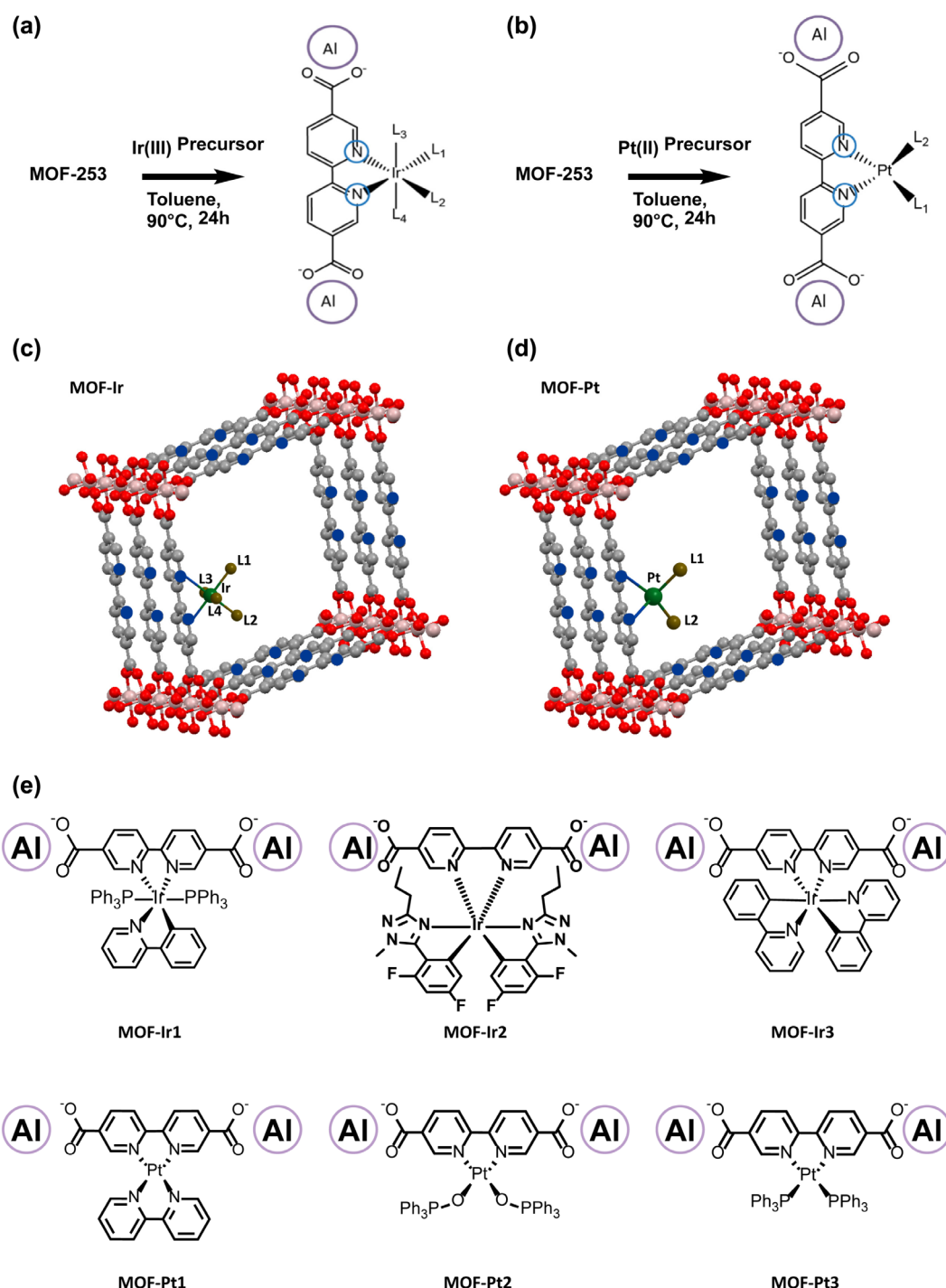
2.2.2. Characterisation techniques

See the Supplemental material.



Scheme 3. Synthetic pathway of Iridium precursor (**Ir3**).





Scheme 4. (Colour online) Schematic representation of synthetic route for MOF Ir(III) complexes (a) and MOF Pt(II) complexes (b); structure of the final materials (c, d); chemical structure of MOF-TMCs system (e).

3. Result and discussion

3.1. Synthesis of MOF host (MOF-253)

MOF-253 was synthesised according to previous literature procedure (27). The further Soxhlet extraction in methanol allows the removal of guest DMF, the reaction solvent, to obtain empty pores. Thermogravimetric analysis shows a single weight loss between 450 and 550 °C,

accounting for 80% of the total starting mass, confirming the expected weight ratio between aluminium oxide and the 22'-bipyridine 55'-dicarboxylate (bpydc) ligand.

In order to assay the crystallinity of **MOF-253**, transmission electron microscopy (TEM) and powder X-ray diffraction (PXRD) analysis have been performed. TEM (not shown) gave a first indication that we have a crystalline material, with micron-sized crystals. The PXRD pattern of

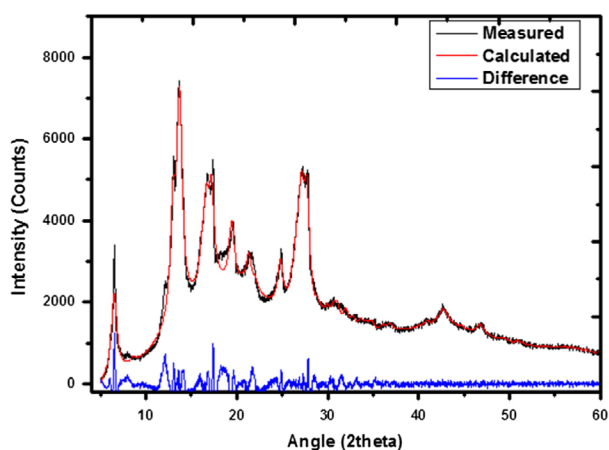


Figure 2. (Colour online) Powder XRD diffractogram of MOF-253.

MOF-253 (Figure 2) resembles the one reported by Yaghi et al., (27) with an orthorhombic crystal phase and a $I\bar{m}ma(74)$ space group. The pore size of the **MOF-253** based on the nitrogen adsorption-desorption measurements is 1.2 nm (see Figure S11). This value is close to the expected length of the linker (22'-Bipyridine-4-4'-dicarboxylate).

3.2. Insertion of Pt(II) and Ir(III) complexes

Bipyridine complexes of some transition metal complexes are known for their good stability and interesting luminescence properties. The 55' dicarboxylate bipyridine of the MOF possess two chelating sites: the carboxylate engaged in the coordination with aluminium ion, while the chelating bipyridine is available for coordinating different metal complex precursors by a ligand substitution between the chloride, of the metal complex precursor, and the 22'-bipyridine moieties, the latter belonging to the framework.

In order to study the effects of the coordination of the bipyridine linker on the structure and photophysical properties of **MOF-253**, a series of Pt(II) and Ir(III) complexes, shown in Scheme 4, were prepared and inserted in **MOF-253**. These two metals in particular were chosen due to their potential emission properties and different geometry and oxidation number. Ir(III) has a d^6 electronic configuration displaying an octahedral geometry, while the d^8 electronic configuration of Pt(II) allows their relative complexes to have a square planar geometry.

To understand the size and charge effect of the guest complexes, we explored different iridium complexes possessing neutral or cyclometallated ligands. The influence of the ligands on the spectroscopic properties is of great importance since it determines the energy (color) of the emission upon coordination to the bipyridine. **Ir1**, bearing two bulky, strong sigma donor, monodentate ligands, triphenylphosphines, was chosen in order to evaluate the

Table 1. Loading ratio of TMC inserted in **MOF-253** by coordination bond.

Material	Non-coordinated bipy (%)	Coordinated bipy (%)
MOF-Ir2	76.06	23.94
MOF-Ir3	58.39	41.61
MOF-Pt1	37.17	62.83
MOF-Pt2	64.46	35.54
MOF-Pt3	66.57	33.43

effect of the steric hindrance during the coordination of Ir(III) complex inside of the MOF pore. **Ir2** was selected because fluorinated groups, shifting the emission to higher energy, have attracted a lot of interest in the literature and is more bulk and **Ir3** but less than **Ir1**. **Ir3** was also used because we had available the known metal complex analogue, $\text{Ir}(\text{ppy})_2(\text{bpy})^+$ (19, 38).

Pt1 and **Pt3** are interesting to compare, since they have a 22-bipyridine and two triphenylphosphine moieties, respectively. Finally, **Pt2** was chosen in order to induce only a structural modification and use it as a reference for the Pt(II) complexes in the MOF.

3.3. XPS analysis

One of the problems related to the insertion of moieties inside MOFs is their quantification. We have therefore devoted much effort to establish if the transition metal complex (TMC), is inserted in the framework of the MOF, through coordination with the bipyridine, but also we have quantitatively evaluated the amount of free ligand and metal complex we have for each system. In order to achieve our goal, we have performed elemental analysis of the MOF-TMC systems and core nitrogen scan using XPS. The obtained elemental atomic ratios from the survey spectra are shown in Table 1, chloride being the counter anion.

The elemental analysis from XPS shows that except for **MOF-Ir1**, all the samples contain both Al and the TMC guest, with a transition metal/Al ratio between 0.2 and 0.5 proving that the samples contain some free ligand in the framework. The **Ir1** precursor is not inserted within the MOF, while for the other iridium complexes we could obtain **MOF-Ir2** and **MOF-Ir3**. This is confirmed by the XPS data, in which the survey does not show aluminium (Table S1, Supplemental material). One possible reason is the disassembly of **MOF-253** during the coordination process because of the steric hindrance, dictated by the bulky phosphines in the octahedral geometry of the complex, which prevent the formation of the MOF. In this case, the isolated product is a crystalline iridium complex possessing bpydc as ancillary ligand.

The XPS core nitrogen high resolution differentiates between the binding energy of coordinated and non-coordinated nitrogen in the bpydc linker. Such energy

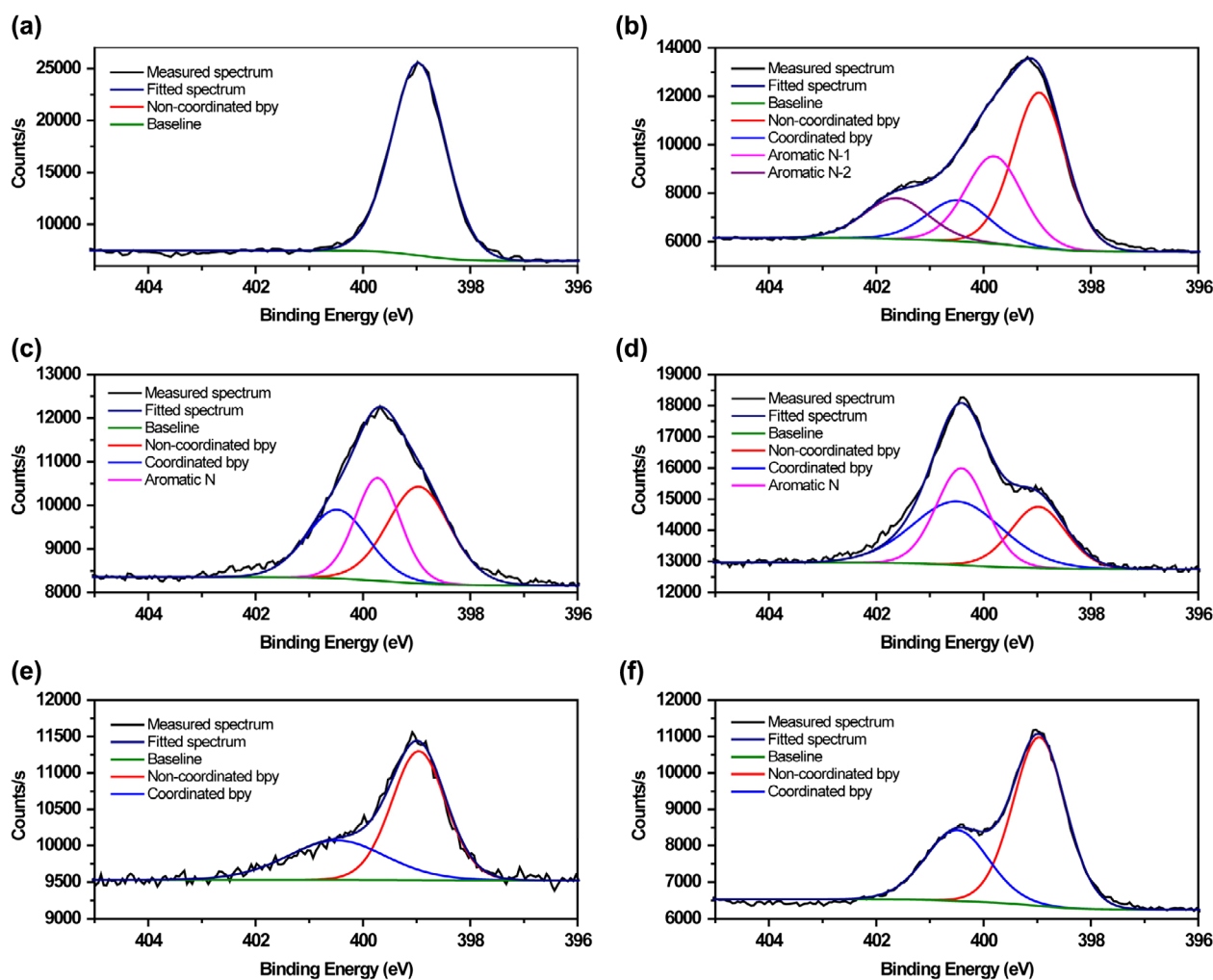


Figure 3. (Colour online) XPS N 1s high resolution spectra of MOF-253 (a), MOF-Ir2 (b) and MOF-Ir3 (c), MOF-Pt1 (d) MOF-Pt2 (e) and MOF-Pt3 (f).

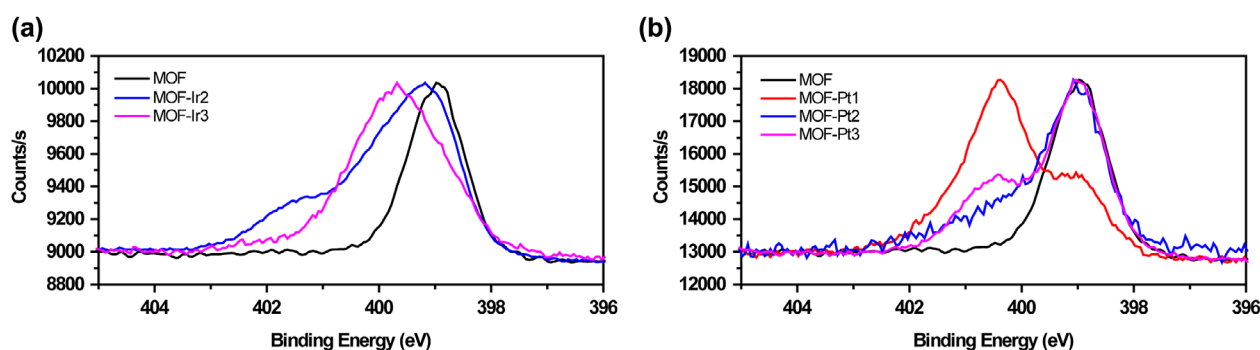


Figure 4. (Colour online) Non-deconvoluted N1s spectra of MOF-253 and MOF-Ir systems (a); and MOF-253 and MOF-Pt systems (b).

difference together with the intensity of the peaks allows us to calculate the amount of free bipyridine for each system. Figure 3 shows respectively XPS N 1s high resolution spectra of **MOF-253** and MOF-Ir(III) systems; as well as of **MOF-253** and MOF-Pt(II) systems. As can be seen for **MOF-253**, we observe, as expected, a single peak for the

22'-bipyridine, with a binding energy of 398.98 eV which matches the reported energy value from literatures for the non-coordinated aromatic nitrogen (39). The MOF-TMCs systems show a more complex band, that after deconvolution process, reveals additional signals at higher binding energy due to the coordination of the 22'-bipyridine to the

transition metal. For instance, high-resolution N scan of MOF-Pt3 shows another signal, at higher binding energy (400.55 eV), meaning that a certain number of N atoms from the MOF framework are coordinated to the metal ion. Regarding MOF-Ir systems and **MOF-Pt1**, since these complexes contain ligands with nitrogens (phenylpyridine, bipyridine, triazole), additional signals are observed and are indicated in the figure as aromatic nitrogen. Such peaks are however important since they further confirm the presence of the metal complex coordinated in the MOF.

From the ratio between the areas of the coordinated and non-coordinated species, Figure 3, we can quantify the loading ratio. For example if we estimate the ratio in the case of MOF-Pt3, (curve f Figure 3), we obtain 33.43% of loading ratio. We are aware that the calculations refer only to several tenths of nanometers from the surface and therefore are not fully corresponding to the all crystal, however the data are reproducible and consistent with the type of metal complex we have inserted. The loading ratios of the TM, calculated by the quantification of each peak, are summarised for all the complexes in Table 1. For clarity, the non-deconvoluted N1s spectra are shown in Figure 4.

As can be seen in Table 1 there is a relationship between the size and the loading of the complexes within the same metal ion, as well as differences between the different metal compounds related to the geometry of them. Indeed MOF-Pt systems should have a higher tendency towards coordination than **MOF-Ir2** and **MOF-Ir3**. This is likely due to the octahedral geometry of Ir(III), which takes more space than the square planar Pt(II) compounds. It is interesting to note that due to the bulkiness of the triphenylphosphine moieties, **MOF-Pt2** and **MOF-Pt3** exhibit a less efficient coordination than the **MOF-Pt1**, bearing a bpy moiety as ancillary chelate. Finally we find as expected that **MOF-Pt2** and **MOF-Pt3** have a similar loading due to a related size, but different emission properties.

3.4. PXRD analysis

The crystallinity of the materials was demonstrated by PXRD analysis. Indeed, they all show evidence of crystallinity (see Supplemental Material) and after refinement and indexing using Total Pattern Analysis Solution (TOPAS) program (40), we were able to determine the crystal phase as well as the space group and the parameters of one unit cell (Table S2). As an example, the PXRD diffractogram of **MOF-Ir2** is shown in Figure 5 in which the simulated PXRD pattern was calculated from the lattice parameters, revealing a striking similarity between both measured and calculated diffractograms (Figure 5, Figure S12 for other MOF system) with relatively low Rwp values. It is important to note that after encapsulation of the TMCs

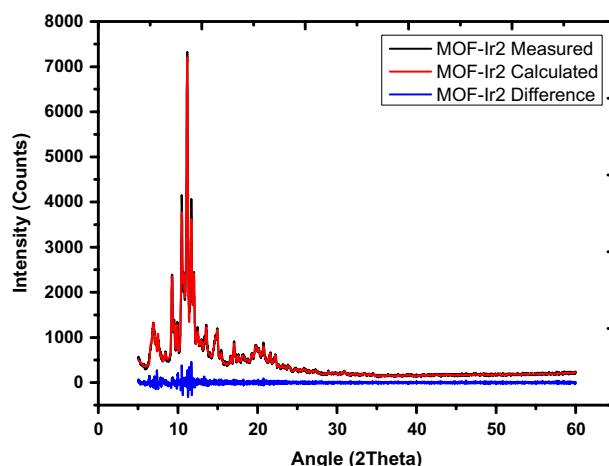


Figure 5. (Colour online) Measured (black) and simulated from TOPAS(red) PXRD diffractograms of **MOF-Ir2**. The difference between the two patterns is in blue.

in the framework of the MOF, the crystal parameters are completely changed due to distortion of the MOF crystal. Indeed, from Table S2, we observe that in comparison with the reference **MOF-253**, which crystallises in an orthorhombic phase, **MOF-Ir2**, **MOF-Pt2** and **MOF-Pt3** crystallise in a monoclinic phase. For the other materials, even though their crystal systems are orthorhombic, their space groups are different, as well as the dimension of one unit cell. Such phenomena have been, indeed, observed by other research groups when guest molecules are entrapped in MOF (41). Interestingly for **MOF-Pt2** and **MOF-Pt3**, which have the same loading and very similar size the distortion is almost identical.

An example of morphology and size of the MOF-TMCs systems is shown in Figure S13. The TEM images show that the crystals have lengths in the micron scale.

3.5. Photophysical properties

After proving the crystallinity of the materials and determining the crystal parameters of each MOF-TMC material, the photophysical properties of the materials were studied. **MOF-253** is a yellow emissive solid, with a photoluminescence quantum yield (PLQY) of 1% and a nanosecond range excited state lifetime. After post-synthetic modification, the emission energy of the final hybrid material is often different from the original MOF. Emission and excitation spectra of **MOF-253** and MOF-TMC species are shown in Figure 6. Interestingly, we can cover the full visible spectrum, going from the blue (470 nm) to the red (616 nm). The luminescence properties of MOF-TMC systems, and the corresponding bipyridine complexes made to compare their properties with the MOF-TMC species, are summarised in Table 2 (Figures S14 and S15).

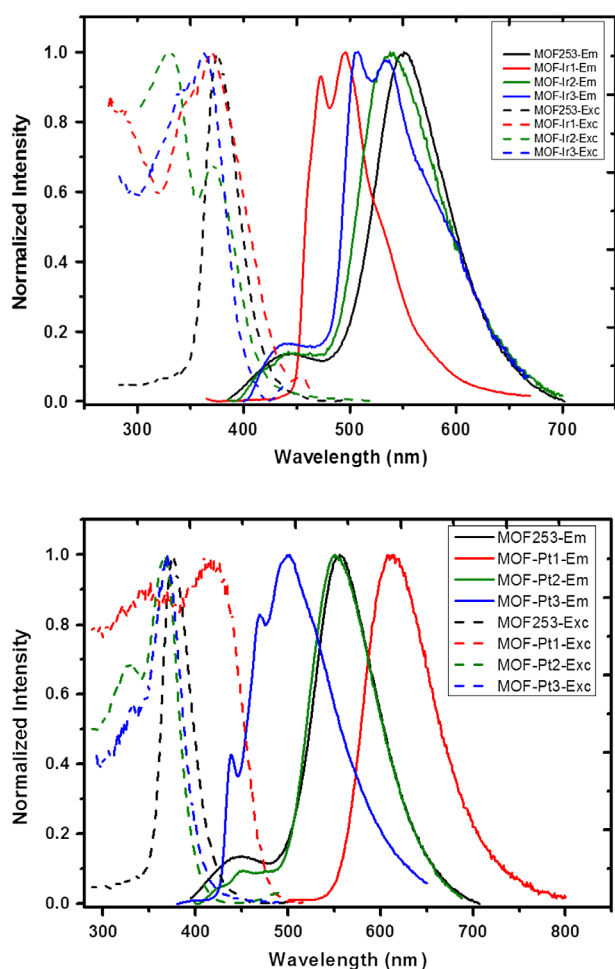


Figure 6. (Colour online) Solid state excitation ($\lambda_{em} = \lambda_{max}$ of emission spectra) and emission ($\lambda_{exc} = 350$ nm) profiles of **MOF-253**, **MOF-Pt** (top) and **MOF-Ir** (bottom) systems.

MOF-253 possesses an emission band at 555 nm and a weak band at 442 nm. The lowest energy emission is attributed to the Al complex (42), which is a perturbed fluorescence of the coordinated carboxylate ligands. The blue emission is tentatively attributed to a residual fluorescence of the non-coordinated bipyridine in the rigid framework. **Ir1** complex displays two bands at 472 nm and 496 nm typical of this Ir(III) compound with excited state lifetimes in the microsecond regime, due to the triplet nature of the emissive excited state. As already mentioned, the **Ir1** precursor cannot form MOF-complex hybrids but coordinate the free bipyridine ligand to form the **Ir1** preventing the formation of the MOF structure. **MOF-Ir2** shows a similar emission profile as the pristine MOF, but a blue shift is observed (see Table 2) and the excited state lifetime of 227 ns is definitely longer than the MOF alone (3–6 ns). The nature of such radiative transition is therefore mainly a triplet metal to ligand charge transfer, 3MLCT , involving the bpy ligand. **MOF-Ir3** also shows a charge transfer emission comparable to the analog $Ir(ppy)_2(bpy)^+$ reported by other

Table 2. Most important photophysical properties of the investigated materials.

Material	λ_{em} , nm	ϕ (%)	τ , ns
MOF-253	555	1	6 (87%)
			3 (13%)
MOF-Ir1	497	3	3087 (82.5%)
			657 (17.5%)
MOF-Ir2	551	1	227 (37%)
			36 (22%)
MOF-Ir3	504	1	3 (41%)
			5367 (53%)
MOF-Pt1	616	3	10 (32.5%)
			3016 (14.5%)
MOF-Pt2	543	5	225 (19.88%)
			10 (24.32%)
MOF-Pt3	470	3	82 (55.80%)
			6 (24%)
Py-Ir3 (Refs. 19, 28)	510, 560	9	3 (76%)
			67 (56%)
Py-Pt1	610	1	4780 (100%)
			2299 (61%)
Py-Pt3	425, 465	1	418 (39%)
			203 (34%)
			8 (66%)

researchers (38, 43), but just few nanometers blue shifted that can be attributed to the rigidochromic effect imposed by the immobilisation of the complex in the MOF structure. Such an effect was already reported by Li et al. (19) for a similar complex. The emission decays bi-exponentially in the microsecond range.

Upon insertion of the Pt(II) precursor, we have a modulation of the emission that spans from blue to red. The **MOF-Pt1** showed a red luminescence ($\lambda_{em} = 616$ nm), and this emission is almost identical to the one of the complexes **Pt1** not linked to the MOF (Pt(II)bis-22'-bipyridine dichloride) (Figure S13). We have attributed this emission to a 3MLCT transition. **MOF-Pt2** displays the same emission profile and the same excited state lifetime as **MOF-253**. Indeed, the complex is a non-emissive species due to the presence of the oxygen on the phosphine (phosphine oxide). Therefore, the only emission that is recorded is the yellow emission of the free site of the **MOF**. Finally, **MOF-Pt3** exhibits an emission higher in energy, showing two bands at 467 and 503 nm. Even though we do not have a clear explanation why we do not see an energy transfer from the metal complex to the MOF the long excited state lifetime can rule out that the high energy emission comes from a singlet excited state (fluorescence of the MOF). We attribute the emission to the presence of the platinum complex and due to the structured emission profile we assign it to a ligand-centred emission. In conclusion, the photophysical properties of the hybrid MOF systems show that in the case in which the emission of the complex is lower in energy than the MOF alone, **MOF-Pt1**, the presence of the metal compound quenches the MOF emission since the coordination occurs on the same ligand and therefore the lowest excited state is populated, like in

an intramolecular energy transfer. However, in all the other systems we do not observe the emission of the framework most likely because of a distortion in the MOF framework, causing non-radiative deactivation.

The emission colours of the crystals can also be observed under a confocal microscope (Figure S16) and the spectrograph gave the same emission profiles as the one reported above.

4. Conclusion

We successfully introduced metal complexes in the MOF framework and were able to tune the luminescence of the MOF-TMC hybrid material. The guest inclusion was performed according to a smart design by a ligand substitution and the formation of coordinative bonds. The characterisations by X-ray photoelectron spectroscopy and powder X-ray diffraction prove the presence of the complex-type guest encapsulation inside the pores of the **MOF-253**. Interestingly a correlation between sizes and geometries of the complexes and their loading in the MOF structures is found, and discussed for the compounds investigated.

Acknowledgment

The authors acknowledge the financial support by the European Union FP7-SACS.

Disclosure statement

No potential conflict of interest was reported by the authors.

Funding

This work was financially supported by the European Union FP7-SACS Project [grant agreement number 2012-310651].

References

- Rowell, J.L.C.; Yaghi, O.M. *Microporous Mesoporous Mater.* **2004**, *73* (1–2), 3–14.
- Gangu, K.K.; Maddila, S.; Mukkamala, S.B.; Jonnalagadda, S.B. *Inorg. Chim. Acta* **2016**, *446*, 61–74.
- Zhoua, H.-C.; Kitagawa, S. *Chem. Soc. Rev.* **2014**, *43*, 5415–5418.
- Tsotsalas, M.; Maheshwari, H.; Schmitt, S.; Heißler, S.; Feng, W.; Levkin, P.A. *Adv. Mater. Interfaces* **2016**, *3* (1), 1500392.
- Mason, J.A.; Veenstra, M.; Long, J.R. *Chem. Sci.* **2014**, *5* (1), 32–51.
- Li, Y.; Yang, R.T. *Langmuir* **2007**, *23* (26), 12937–12944.
- Zhao, Z.; Ma, X.; Kasik, A.; Li, Z.; Lin, Y.S. *Ind. Eng. Chem. Res.* **2012**, *52* (3), 1102–1108.
- Horcajada, P.; Chalati, T.; Serre, C.; Gillet, B.; Sebrie, C.; Baati, T.; Eubank, J.F.; Heurtaux, D.; Clayette, P.; Kreuz, C.; Chang, J.-S.; Hwang, Y.K.; Marsaud, V.; Bories, P.-N.; Cynober, L.; Gil, S.; Férey, G.; Couvreur, P.; Gref, R. *Nat. Mater.* **2010**, *9* (2), 172–178.
- McKinlay, A.C.; Morris, R.E.; Horcajada, P.; Férey, G.; Gref, R.; Couvreur, P.; Serre, C. *Angew. Chem. Int. Ed.* **2010**, *49* (36), 6260–6266.
- Rowe, M.D.; Thamm, D.H.; Kraft, S.L.; Boyes, S.G. *Biomacromolecules* **2009**, *10* (4), 983–993.
- Tsotsalas, M.; Liu, J.; Tettmann, B.; Grosjean, S.; Shahnas, A.; Wang, Z.; Azucena, C.; Addicoat, M.; Heine, T.; Lahann, J.; Overhage, J.; Bräse, S.; Gliemann, H.; Wöll, C. *J. Am. Chem. Soc.* **2014**, *136* (1), 8–11.
- Wang, C.; Wang, J.L.; Lin, W. *J. Am. Chem. Soc.* **2012**, *134* (48), 19895–19908.
- Allendorf, M.D.; Schwartzberg, A.; Stavila, V.; Talin, A.A. *Chem. Eur. J.* **2011**, *17* (41), 11372–11388.
- Wu, J.; Zhang, H.; Du, S. *J. Mater. Chem. C* **2016**, *4* (16), 3364–3374.
- Liu, J.J.; Shan, Y.B.; Fan, C.R.; Lin, M.J.; Huang, C.C.; Dai, W.X. *Inorg. Chem.* **2016**, *55* (7), 3680–3684.
- Rao, X.; Huang, Q.; Yang, X.; Cui, Y.; Yang, Y.; Wu, C.; Chen, B.; Qian, G. *J. Mater. Chem.* **2012**, *22* (7), 3210–3214.
- Serre, C.; Millange, F.; Thouvenot, C.; Gardant, N.; Pelle, F.; Férey, G. *J. Mater. Chem.* **2004**, *14* (10), 1540–1543.
- Allendorf, M.D.; Bauer, C.A.; Bhakta, R.K.; Houk, R.J. *Chem. Soc. Rev.* **2009**, *38* (5), 1330–1352.
- Sun, C.-Y.; Wang, X.-L.; Zhang, X.; Qin, C.; Li, P.; Su, Z.-M.; Zhu, D.-X.; Shan, G.-G.; Shao, K.-Z.; Wu, H.; Li, J. *Nat. Commun.* **2013**, 1–8.
- Lulf, H.; Bertucci, A.; Septiadi, D.; Corradini, R.; De Cola, L. *Chem. Eur. J.* **2014**, *20* (35), 10900–10904.
- de Barros e Silva Botelho, M.; Fernandez-Hernandez, J.M.; de Queiroz, T.B.; Eckert, H.; De Cola, L.; de Camargo, A.S.S. *J. Mater. Chem.* **2011**, *21* (24), 8829–8834.
- Kim, Y.Y.; Carloni, J.D.; Demarchi, B.; Sparks, D.; Reid, D.G.; Kunitake, M.E.; Tang, C.C.; Duer, M.J.; Freeman, C.L.; Pokroy, B.; Penkman, K.; Harding, J.H.; Estroff, L.A.; Baker, S.P.; Meldrum, F.C. *Nat. Mater.* **2016**, *15*, 903–910.
- Sadakiyo, M.; Yamada, T.; Kato, K.; Takata, M.; Kitagawa, H. *Chem. Sci.* **2016**, *7* (2), 1349–1356.
- Mukherjee, S.; Joarder, B.; Manna, B.; Desai, A.V.; Chaudhari, A.K.; Ghosh, S.K. *Sci. Rep.* **2014**, *4*, 1–7.
- Zhenqiang Wang, S.M.C. *J. Am. Chem. Soc.* **2007**, *129*, 12368–12369.
- Gadzikwa, T.; Farha, O.K.; Mulfort, K.L.; Hupp, J.T.; Nguyen, S.T. *Chem. Commun. (Camb.)* **2009**, *25*, 3720–3722.
- Bloch, E.D.; Britt, D.; Lee, C.; Doonan, C.J.; Uribe-Romo, F.J.; Furukawa, H.; Long, J.R.; Yaghi, O.M. *J. Am. Chem. Soc.* **2010**, *132* (41), 14382–14384.
- Wang, M.; Yuan, B.; Ma, T.; Jiang, H.; Li, Y. *RSC Advances* **2012**, *2* (13), 5528–5530.
- Liu, H.; Yin, B.; Gao, Z.; Li, Y.; Jiang, H. *Chem. Commun. (Camb.)* **2012**, *48* (14), 2033–2035.
- Carson, F.; Agrawal, S.; Gustafsson, M.; Bartoszewicz, A.; Moraga, F.; Zou, X.; Martin-Matute, B. *Chem. Eur. J.* **2012**, *18* (48), 15337–15344.
- Vezzu, D.A.K.; Deaton, J.C.; Jones, J.S.; Bartolotti, L.; Harris, C.F.; Marchetti, A.P.; Kondakova, M.; Pike, R.D.; Huo, S. *Inorg. Chem.* **2010**, *49* (11), 5107–5119.
- Miskowski, V.M.; Houlding, V.H. *Inorg. Chem.* **1989**, *28* (8), 1529–1533.
- Aliprandi, A.; Mauro, M.; De Cola, L. *Nat. Chem.* **2016**, *8* (1), 10–15.

- (34) Mauro, M.; Aliprandi, A.; Cebrian, C.; Wang, D.; Kubel, C.; De Cola, L. *Chem. Commun. (Cambridge, U. K.)* **2014**, 50 (55), 7269–7272.
- (35) Wu, S.-H.; Ling, J.-W.; Lai, S.-H.; Huang, M.-J.; Cheng, C.H.; Chen, I.C. *J. Phys. Chem. A* **2010**, 114 (38), 10339–10344.
- (36) Eum, M.-S.; Chin, C.S.; Kim, S.Y.; Kim, C.; Kang, S.K.; Hur, N.H.; Seo, J.H.; Kim, G.Y.; Kim, Y.K. *Inorg. Chem.* **2008**, 47 (14), 6289–6295.
- (37) Garces, F.O.; King, K.A.; Watts, R.J. *Inorg. Chem.* **1988**, 27 (20), 3464–3471.
- (38) Mauro, M.; De Paoli, G.; Otter, M.; Donghi, D.; D'Alfonso, G.; De Cola, L. *Dalton Trans.* **2011**, 40 (45), 12106–12116.
- (39) Jansen, R.J.J.; van Bekkum, H. *Carbon* **1995**, 33 (8), 1021–1027.
- (40) Coelho, A.A. *J. Appl. Cryst.* **2003**, 36, 86–95.
- (41) Raatikainen, K.; Rissanen, K. *Chem. Sci.* **2012**, 3 (4), 1235–1239.
- (42) Goswami, M.; Nayak, P.K.; Periasamy, N.; Madhu, P. *Chem. Cent. J.* **2009**, 3 (1), 15.
- (43) Ladouceur, S.; Zysman-Colman, E. *Eur. J. Inorg. Chem.* **2013**, 2013 (17), 2985–3007.